Chapter 5: Degradation of *p*-cresol in the presence of UV light driven in an integrated system containing photocatalytic and packed bed biofilm reactor

The content that is included in this chapter has been published.

Jaiswal, V.K., Gupta, A.D., Verma, V., Singh, R.S., 2023. Bioresource Technology Degradation of p-cresolin the presence of UV light driven in an integrated system containing photocatalytic and packed bed biofilm reactor. Bioresour. Technol. 387, 129706.
https://doi.org/10.1016/j.biortech.2023.129706

5.1. Introduction

Water pollution has emerged as one of the world's most pressing problems due to rapid industrial growth and seriously threatens ecosystems and human health (Zhou et al., 2017; Liu et al., 2017). Phenolic wastewater is produced during coal coking, coal gas purification, chemical recovery, and refining crude oil. It comprises phenols and their derivatives, PAHs (polycyclic aromatic hydrocarbons), and other persistent organic molecules (Qu et al., 2022). 4-methyl phenol (*p*-cresol) is a significant volatile phenolic compound (Sundaresan et al., 2021). The US EPA (U.S. Environmental Protection Agency) has designated it as one of the priority pollutants (Khunphonoi and Grisdanurak, 2016), showing chronic effects at 12 mg L^{-1} of the quantitative structure-activity relationship (Flox et al., 2009). *p*-Cresol adversely affects human skin, eyes, respiratory system, mood, and mental health even at low concentrations when exposed to it over a prolonged period (Singh et al., 2017). It is moderately soluble and stable in water. According to the WHO, 0.001 mg L^{-1} of *p*-cresol is permitted in potable water (Panigrahy et al., 2020). Hence, *p*-cresol effluent must undergo thorough treatment before being discharged into the environment. In the earlier days, various advanced oxidation processes (AOPs) and biological methods were developed to degrade *p*-cresol (Alkathiri et al., 2020). AOPs are superior to conventional wastewater treatment methods because of their non-selectivity and excellent redox potential of free radicals on the removal of persistent pollutants (Kakavandi and Babaei, 2016). The most common AOPs include sonolysis, ozonation, electrochemical oxidation, photocatalysis, and photo-Fenton (Tiwari et al., 2022). To degrade recalcitrant molecules in an aqueous solution, photocatalysis has received much attention (Takdastan et al., 2018). Photocatalytic oxidation strategies using ultraviolet (UV) light and transition metal as photocatalysts, such as titanium dioxide (TiO_2) and zinc oxide (ZnO), have been developed in recent years and have attracted a lot of attention from researchers as an advanced wastewater purification technology due to their effectiveness at decomposing and mineralizing toxic chemical pollutants (Zamri and Sapawe, 2019). Nonetheless, TiO_2 is seen as a potentially practical alternative to the several photocatalysts that are currently used. TiO_2 has been widely employed for various applications because of its inexpensive cost, non- toxic qualities, chemical reaction stability, and photo-corrosion resistance (Li et al., 2012). TiO_2 produces electrons and holes under the influence of UV light, which promotes the generation of free radicals that effectively oxidize pollutants

(Dhanya and Aparna, 2016). However, AOPs have several disadvantages, including incomplete degradation, the creation of hazardous intermediates, high operating costs, and high disposal costs for waste sludge (Singh et al., 2017). In contrast, biological methods are promoted as economical and environmentally beneficial for degrading a wide range of pollutants (Bharti et al., 2019). Unfortunately, the biodegradation process is ineffective because of the high concentration of contaminants and the toxicity of such compounds to microorganisms (Zhang et al., 2010). Photocatalysis depends on UV irradiation in combination with photocatalysts to generate free radicals, while biodegradation highly depends on enzymatic degradation processes using oxidoreductive enzymes (Waghmode et al., 2019). The challenges of AOPs and biological processes may be overcome by integrated photocatalytic- biological degradation. In this integral approach, photocatalysis transforms hazardous organics into biodegradable products successfully mineralized through biodegradation (Ma et al., 2015). Combining photocatalysis with biodegradation offers significant advantages, including more comprehensive and rapid degradation of most pollutants, along with potential economic viability, environmental friendliness, and sustainability (Zhang et al., 2021). Based on the literature survey, very few attempts have been made to create an integrated system (Photocatalysis and biodegradation) for *p*-cresol wastewater treatment. In this work, a photocatalytic reactor is followed by PBBR to examine the performance of a hybrid system. The preparation of the photocatalyst and morphology, shape, size, and crystallinity were investigated. Also, the effects of pH, TiO_2 dosage, and concentration were investigated. The PBBR performance was evaluated in terms of % removal (REp), pollutant loading rate (PLR), and % elimination capacity (ECPR).

5.2. Materials and methods

5.2.1. Chemicals

In this present study, *p*-cresol (99%) and MSM (Mineral salt medium) were prepared as per the methods given in **Chapter 3 (Section 3.2.1)** in detail.

5.2.2. Acclimatization of bacterial culture, isolation and bacterial identification

The acclimatization and isolation technique used in this study has been discussed in previous studies (Jaiswal et al., 2023). The acclimatization followed the detailed methodology provided **Chapter 3 (Section 3.2.2)**. The serial dilution method was used to obtain pure strain. Triyat

Scientific in Nagpur, India, characterized the viable bacterial species by amplifying the DNA using polymerase chain reaction (PCR) with universal forward (27F-5′ GGATGAGCCCGGCCTA3′) and reverse (11492R-5′ CGGTGTGTACAAGGCCCGG3′) primers. Bacterial consortia (*Serratia marcescens* strain HL 1 and *Ochrobactrum intermedium*) were used for biodegradation of *p*-cresol. The details of bacterial consortia are discussed in the Appendix **(Appendix 5 (a, b)).**

5.2.3. Analytical methods

The concentration of bacterial cells and residual-cresol concentration were analysed as per the details given in **Chapter 3 (Section 3.2.4)**. The BOD value was calculated using protocol (Apha, 1998). The COD was analyzed by using UNIPHOS COD DIGESTER. The TOC analyzer (multi-N/C 2100/2100S, Analytikjena, Germany) was used to evaluate the sample. The functional group of photos catalytically oxidized and the biodegraded sample was determined using Fourier transform infrared spectroscopy (FTIR) (Nicolet iS5, THERMO with 4 cm^{-1} resolution, 4000–500 cm^{-1} frequency range, 32 numbers of scan).

5.2.4. Synthesis of TiO_2 nanoparticles

The approach used to synthesize TiO_2 nanoparticles in this study has been reported elsewhere (Saroj et al., 2020). Briefly, the solution- combustion method was used to create TiO_2 photocatalysts. Titanium (IV) dioxide (TiO_2) (0.063 mol) and ammonium sulphate ($(NH_4)_2SO_4$) (0.378 mol) were in a 1:6 ratio and dissolved in 100 mL of 98% pure H_2SO_4, accordingly. The mixture was stirred at 170 ^oC for 2 to 3 h on a hot plate cum stirrer at 400 rpm to produce titaniumoxysulphate $TiO(SO_4)$. The total volume of the mixture was increased to 500 mL by adding Milli-Q water. The resulting slurry was neutralized (pH 7) by gradually adding 25% ammonium solution. After the neutralization, a milky white precipitate developed, and it was filtered using a Buchner funnel and dissolved in 98 % pure HNO_3 and 10 g citric acid was added. The resulting mixture evaporated at 70–80 °C on a hot plate while constantly agitated until it spontaneously ignited. The combination produced an extremely fine crystalline residue at evaporating temperatures. Citric acids behave as a complex-forming agent in the ignition, forming a complex compound by reacting with cations and producing combustion fuel. After that, TiO_2 nanoparticles were produced by calcinating the crystalline residue at 500 °C for 5 h.

5.2.5. Characterization of synthesized TiO_2 nanoparticles

Field emission scanning electron microscopy (SUPRA 55VP) was used to examine the shape and structure of the particles. The XPS analysis was used to investigate the chemical state and binding energy of ions in the synthesized photocatalysts by using monochromated Mg-K (1253.6 eV) as the X-ray source (AMICUS, Kratos Analytical, England). X-ray diffraction (XRD) (Brukur D8 Advance AXS) with CuKα radiation (1.5406 Å) in the 2θ scan range of 20-70° was used to investigate the crystallinity of TiO_2 nanoparticles. The size of nanoparticles was measured by ImageJ software.

To evaluate the antibacterial activity of titanium oxide (TiO_2) nanoparticles, Gram-positive Staphylococcus aureus (*S. aureus*) and Gram-negative Escherichia coli (*E. coli*) bacteria strains were chosen. ATCC (American Type Culture Collection) was the source of the microorganisms. The antimicrobial activity of synthesized TiO_2 nano particles was investigated using the well diffusion method. Nutrient agar medium (20 mL) was poured into sterile Petri dishes, followed by the addition of 2 mL of seeded medium previously inoculated with bacteria. The plate was perforated (7.4 mm in diameter) as wells into which TiO_2 nanoparticle powder was loaded. The zone of inhibition was recorded and measured 15 h after incubation at 37 ℃ using ImageJ software.

5.2.6. Photocatalytic reactor

The photocatalytic reactor was constructed from a cylinder of plexiglass with an inside diameter of 2.5 cm and a height of 65 cm, illuminated by UV lamps (Philips TUV 8 W G8T5 Hg, 2537Ao) **(Fig. 5).** The magnetic stirred was employed for consistent nanoparticle dispersion within the reactor. The system was covered with an insulated jacket to prevent interference from outside visible light. For efficient mixing of photo catalyst and *p*-cresol in the solution, only 50 mL of *p*-cresol solution was added to the reactor to the reactor throughout the photodegradation process.

5.2.7. Biodegradation experiment for *p*-cresol degradation

A packed bed biofilm reactor (PBBR) was fabricated of borosilicate glass with a height of 60 cm and inner diameter of 5.5 cm with a working capacity of 1.2 L. Pre sterilized PUF (1 cm × 1 cm × 1 cm) was used as carrier for microorganism's immobilization due to its high porosity with

strong resistance to water adsorption (Mulla et al., 2013). PBBR was run for 15 days in batch mode along MSM as a nutrient source for microorganisms and *p*-cresol (50 mg L^{-1} to 100 mg L^{-1}) as a carbon source under aerobic conditions for the proper formation of biofilm on the carrier. Air constant volumetric flow rate (1 L min^{-1}) was maintained by using rotameter (Flow point, India). A peristaltic pump (ELECTROLAB, PP- 50 V) was used to supply *p*-cresol solution at various flow rates to the reactor. pH (7±0.5) and dissolved oxygen (DO 6±0.5 mg L^{-1}) within the reactor were measured by using a pH meter (HD 2305.0; Delta HM; Italy) and DO meter (HD 2109.1; Delta OHM; Italy) **(Fig. 5.1.).** A constant temperature of 30±2 ˚C was used during degradation. The performance of PBBR was evaluated based on % removal efficiency (REp), elimination

The % removal efficiency of *p*-cresol (RE_p) = $\frac{C_{ip}-C_{op}}{C_{ip}} \times 100$……..……..(5.1)

Elimination capacity of PBBR (EC_{PR}) (mg $L^{-1}d^{-1}$) = $\frac{C_{ip}-C_{op}}{V_R} \times 100$……..……..(5.2)

Pollutant loading rate (PLR) (mg $L^{-1}d^{-1}$) = $\frac{Q_{ip} \times C_{ip}}{V_R}$……..……..(5.3)

where, C_{ip} and C_{op} are inlet and outlet concentrations of *p*-cresol (mg L^{-1}), V_R working volume of the reactor (L), Q_{ip} the influent flow rate in the PBBR (mL h^{-1})

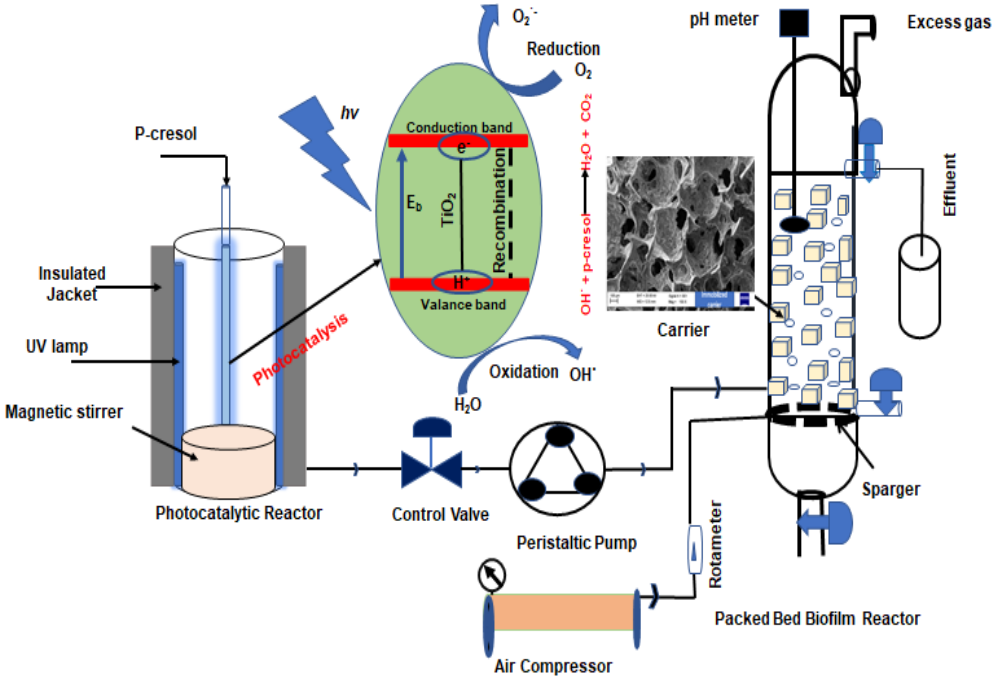

Fig. 5.1. Systematic diagram photocatalytic reactor followed by packed bed biofilm reactor

5.2.8. Photocatalytic kinetic and mechanism for *p*-cresol degradation

The kinetics of the photocatalytic degradation process were examined using the fundamental relationships between kinetics and Langmuir-Hinshelwood. The concentration of intermediate products, rate constants, were calculated through mathematical-chemical modeling by taking the logarithm of the kinetic-based relationship. **Eq. (5.4).**

$$r = \frac{dC_p}{dt} = k \times C^n \quad \text{.....(5.4)}$$

taking log on both sides

$$log\left(\frac{dC_p}{dt}\right) = log\ k + n\ log(C) \quad \text{.....(5.5)}$$

C (mg L^{-1}) is the *p*-cresol concentration, t (min) is photocatalytic reaction time, n is the reaction order, and k is the kinetic constant.

To study the kinetics of photocatalytic processes, Langmuir-Hinshelwood developed a model defined as **Eq (5.6).**

$$r = -\left(\frac{dC}{dt}\right) = \frac{K_r K_a C}{1 + K_a \times C} \quad \text{.....(5.6)}$$

Where, K_r (min^{-1}), K_a and C (mg L^{-1}) is the rate constant, absorption constant and concentration of *p*-cresol, respectively and t (sec) is the reaction time. If the absorption or concentration is low, **Eq. (5.7)** is obtained by simplifying and solving the differential **Eq. (5.6):**

$$r = -\frac{dC_p}{dt} = k_{ap} \times C_p \quad \text{..... (5.7)}$$

Integrating the equation with the following restriction $C_p = C_{p0}$ at $t = 0$, with C_{p0} being the initial concentration of the *p*-cresol solution and t the reaction time, yields the following expression:

$$ln\left(\frac{C_{p0}}{C_p}\right) = k_{ap} \times t \quad \text{..... (5.8)}$$

The expression k_{ap} is the apparent pseudo-first-order rate constant and is affected by the concentration of *p*-cresol.

Using **Eq. (5.9),** the half-life of *p*-cresol at different concentrations was evaluated

$$t_{\frac{1}{2}} = \frac{ln2}{K_{ap}} \quad \text{.....(5.9)}$$

5.2.8.1. Growth and inhibition kinetics model for biodegradation of *p*-cresol

p-Cresol is a widely recognized toxic substance that inhibits the growth of various microorganisms. Several suggested substrate inhibition models show the growth of

microorganisms in a batch reactor in the presence of an inhibitory substrate. Monod and Andrew-Haldane models are two of the most frequently used models for bio-kinetic study. This study uses the Monod model **(Eq. (5.10))** to predict the biodegradation response under non-inhibitory conditions.

$$q = \frac{q_{max} \times S}{s + K_S} \quad \text{.....(5.10)}$$

Monod model is suitable for microbial growth kinetics at low substrate (*p*-cresol) concentrations, but owing to the substrate inhibitory effect, it does not provide adequate results at higher substrate concentrations (Carvajal et al., 2018). However, Andrew-Haldane model was used to study the growth inhibition kinetic of *p*-cresol on biomass using **Eq. (5.11).**

$$q = \frac{q_{max} \times S}{K_S + s + \frac{s^2}{K_I}} \quad \text{.....(5.11)}$$

In the equation above, *S*, K_s, and K_I stand for substrate concentration, half-saturation constant, and inhibition constant (all in mg L^{-1}), and q (h^{-1}), q_{max} (h^{-1}) are the specific *p*-cresol biodegradation rate and maximum specific *p*-cresol biodegradation rate. The estimation of the kinetic parameters, such as K_s and K_I and q_{max} was done using the least- square error technique. By applying this approach, the data are best fitted with kinetics. According to **Eq. (5.12)**

$$\hat{q} = \frac{q_{max}}{1 + {}^{2*}\sqrt{\frac{k_S}{k_I}}} \quad \text{.....(5.12)}$$

$\hat{q}$ refers to the highest possible q during inhibition

5.2.8.2. Statistical analysis

The graphs are shown with standard deviation errors and all the data was provided as Mean ±STDEV (Standard Deviation). Using GraphPad Prism software (version 5.03), the experimental data were analyzed using Dennett's multiple compression test and one-way ANOVA test analysis for variance ($p \leq 0.005$).

5.3. Results and discussion

5.3.1. Characterization of synthesized TiO_2 nanoparticles

5.3.1.1. Field emission scanning electron microscopy analysis of TiO_2 nanoparticles

To calculate the size of the synthesized nanoclusters, the surface morphology of the samples was scanned using the FESEM **(Fig. 5.2.(a)).** The micrograph exhibits nanoscale TiO_2 particles with

nanoparticle and micro-sphere surface shapes. The nanoparticles are distributed in spherical clusters with 32.78 nm-sized. Keshari et al. (2022) prepared nanoparticles using $TiCl_4$ precursor annealed at different temperatures (300, 600, and 900 °C) and found that the average diameter of nanoparticles was 28.12 nm at 900 °C. However, Nadzirah et al. (2015) prepared TiO_2 nanoparticles at different annealed temperatures (400, 500, 600, 700, and 900 °C) and found an average diameter of 11.9 to 61.5 nm.

5.3.1.2. Morphology analysis of TiO_2 nanoparticles

Fig. 5.2.(d) illustrates the X-ray diffraction pattern of synthesized TiO_2 nanoparticles. The diffraction pattern was observed at 2θ values between 20 and 70. Strong diffraction peaks at 27.81° show the wave functions of the electronic eigenstates of the Ti-O-Ti-O chain on the TiO_2/H_2O interface (Rajakumar et al., 2012) and 69.23° indicate an anisate phase with the tetragonal structure of TiO_2 nanoparticles (Lal et al., 2021).

5.3.1.3. X-ray photoelectron spectroscopy analysis of TiO_2 nanoparticles

X-ray photoelectron spectroscopy (XPS) was carried out to analyze the electronic state Ti and O elements of synthesized TiO_2 photocatalyst. **Fig. 5.2.(e)** shows the Ti 2p XPS TiO_2 nanoparticles. The binding energies (BE) of the Ti 2p1/2 and Ti 2p3/2 XPS spectra for the TiO_2 nanoparticles were 458.6 and 464.36 eV, respectively, and the resultant change in BE value between the two peak types (BE =BE (Ti 2p1/2) – BE (Ti 2p3/2)) was 5.76 eV. These features are characteristic of the Ti^{4+}-O bonds in TiO_2 (Chen et al., 2020). **Fig. 5.2.(f)** illustrates the high-resolution O 1s XPS spectra of TiO_2 nanoparticles: Asymmetric peaks at around 529.88 and 531.66 eV, corresponding to the Ti^{4+}-O bond and surface hydroxyl groups (Ti-OH bonds), accordingly (Arunmetha et al., 2021). Khunphonoi and Grisdanurak (2016) observed similar types of XPS spectra using titanium nanorod to degrade *p*-cresol under UV–visible irradiation.

5.3.2. Antibacterial properties of synthesized TiO_2 nanoparticles

The results showed that the synthesized nanoparticle powder exhibited intense antibacterial activity against Gram-negative *Escherichia coli* and Gram-positive *Staphylococcus aureus*. The average zone of inhibition of nanoparticles was 5.1 mm for *E. coli* and 6.4 mm for *S. aureus*. The zone of inhibition of nanoparticles was also compared to the standard antibiotics drug **(Appendix 5 (c)).** However, this study also demonstrated that the TiO_2 nanoparticles exhibited

better activity in Gram-positive bacteria than the Gram-negative bacteria due to an additional outer coat of lipopolysaccharide and the peptidoglycan layer in Gram-negative bacteria that aids in minimizing any potential harm from nanoparticles.

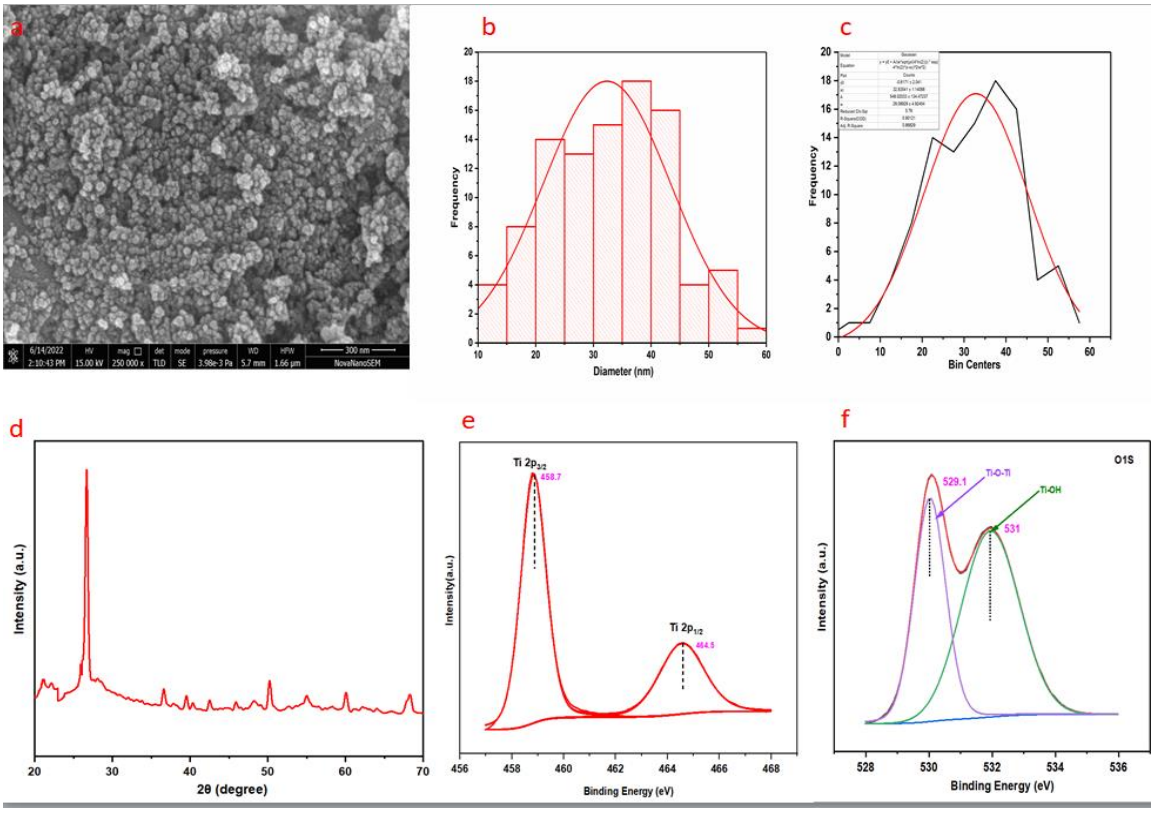

Fig. 5.2. Characterization of synthesized TiO_2 nanoparticle (a) Surface morphology analysis by FESEM, (b, c) Diameter measured by ImageJ software, (d) Crystallinity analysis by XRD, and (e, f) Chemical states of the Ti and O elements analyzed by XPS

5.3.3. Photocatalytic oxidation of *p*-cresol

Fig. 5.3. illustrates the effect of irradiation time on the biodegradability index (BOD_5/COD) and BOD_5/TOC. Higher BOD_5/TOC value shows increased BOD concentrations and less oxidation of organic content in the specific wastewater (Grossule et al., 2022). The initial biodegradability indices of 0.09±0.03 for BOD_5/COD and 0.27±0.05 for BOD_5/TOC observed for a concentration of 700 mg L^{-1} of *p*-cresol suggest that *p*-cresol exhibits poor biodegradability. As irradiation time increases (0–300 min) biodegradability index continuously increases from 0.098±0.03 to 0.59±0.01 for BOD_5/COD and BOD_5/TOC from 0.27±0.05 to 1.74±0.07 **(Fig. 5.3.).** BOD_5/TOC ratio is 1.2–2.0, indicating that waste water contains biodegradable organic matter (Kim et al.,

2022). The results reflect that pre-oxidized *p*-cresol solution has some intermediate product that helps enhance the solution's biodegradability. The photocatalytic degradation process increases the biodegradability index and some extent, % removal. Segura Ceniceros et al. (2003) used ozonation to improve the biodegradability index of 2, 4-dichlorophenol 0.25–0.48 and % removal of TOC 68%. The % removal of *p*-cresol by photocatalysis may be described as follows. Excitation of the photocatalyst by UV light on the reaction mixture generates an electron (e^-) and hole (h^+) in the conduction band (CB) and valance band (VB), respectively. The conversion of air oxygen into a superoxide radical anion ($O2^{\bullet}$) is made possible by transporting electrons from the CB to the catalyst and avoiding the recombination of the excitons. $O_2^{\bullet}$ reacts with protons (H^+) to form peroxide radicals ($HO_2^{\bullet}$) However, the reaction between peroxide radicals and electrons (e^- (CB)) and protons (h^+ (VB)) form hydrogen peroxide. Furthermore, H_2O_2 reacts with e^- (CB) and forms hydroxyl radicals. As well as, holes directly react with OH^- ions to form hydroxyl radicals. Finally, •OH reacts with *p*-cresol and converts final products.

$$p\text{-cresol} + HO^{\bullet} \rightarrow \text{Intermediate product} + CO_2 + H_2O$$

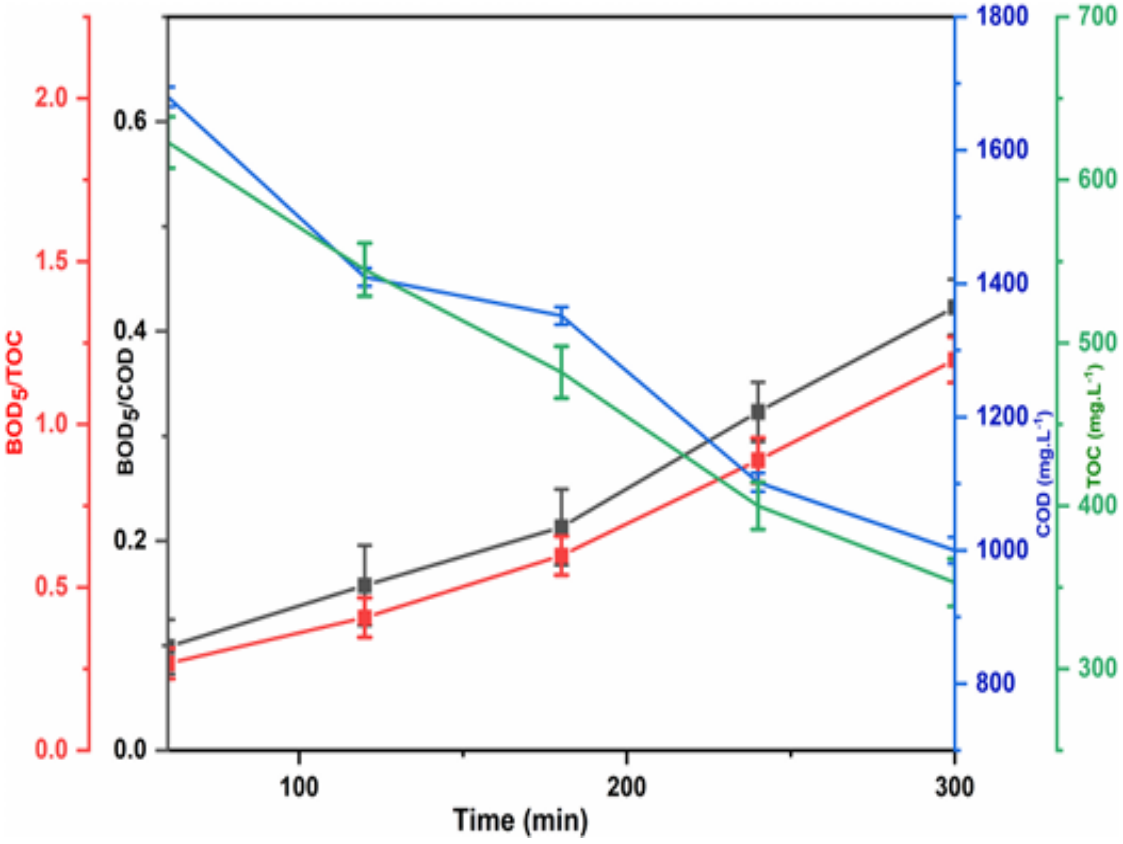

Fig 5.3. Biodegradability index of *p*-cresol (700 mg L^{-1}) pH 3, catalyst dose 1.2 g L^{-1}, irradiation time 300 min

5.3.4. Effect of pH on photocatalytic degradation of *p*-cresol

The aqueous solution's pH affects the photocatalysts surface charge, pollutant degradation rate, pollutants adsorption on the photocatalysts surface, oxidation and reduction potential of the valance band and conduction band (Hosseini et al., 2018). Because the pH of industrial effluent varies, it is essential to investigate how pH affects the photo catalytic process. The effect of pH on photocatalytic degradation of *p*-cresol using TiO_2 nanoparticles was observed in varying pH ranges (1.0 to 10.0) at fixed concentration: 100 mg L^{-1}; catalyst dose: 0.5 g L^{-1}, and irradiation time 300 min **(Appendix 5 (d)).** % RE_P increases with increasing pH (1–3), and the maximum % RE_P of 60.90 ± 2.03% was found to be optimum at a pH of 3. Further, an increase in pH (3 to 10) % RE_P continuously decreases (60.90±2.03 to 24.48±1.23%). Previously, it was studied that the point of zero charge (PZC) for anatase TiO_2 was 6.3 (Lou et al., 2022). When the pH 6.3 surface of Titania is deprotonated according to **Eq. (5.14)** and **(5.15)**

$TiOH + H^+ \rightarrow TiOH^+_2$…… (5.13)

$TiOH + OH^- \rightarrow TiO^- + H_2O$…… (5.14)

According to **Eq. (5.13)** and **(5.14),** in acidic and alkaline circumstances, the surface of Titania bears both positive and negative charges. However, TiO_2 exhibits high oxidizing ability at lower pH. Still, excessive H^+ ions occupied the outer surface of the photocatalyst, which delayed the production of the •OH radical and decreased their rate of reactions (Singh et al., 2022). Nevertheless, under an alkaline environment, coulombic repulsion between the negative TiO_2 and organic compound anions induced substantially reduced contact, decreasing photocatalytic activity.

5.3.5. Effect of doses on photocatalytic degradation *p*-cresol

The catalyst dose used is another one of the most important factors influencing photocatalytic effectiveness and cost. A suitable dose of photocatalyst has the potential to offer the maximum active surface area for the absorption of pollutants. However, an excessive dose may lead to agglomeration of the catalyst, which prevents UV/visible light penetration (Chen et al., 2020). The dose effect on % REp was observed at 0.20 g L^{-1} to 1.5 g L^{-1} **(Appendix 5 (e)).** The % REp was increased when the photocatalytic dose was increased from 0.2 g L^{-1} to 1.2 g L^{-1}, and the maximum % REp (98.43±1.23%) was found at 1.2 g L^{-1}. This was because of active sites' increased formation and photo catalyst loading, which improved •OH radical production. Also,

when the number of photocatalyst particles increased, the number of adsorbed *p*-cresol molecules increased, enhancing the % REp. It was observed that when the photocatalyst dose increased far beyond the 1.2 g L^{-1}, the degree of % REp slightly decreased (98.43±1.23% to 98.13±1.56%). This behaviour may be caused by increased turbidity and less light penetration into the solution (Tiwari et al., 2022). Zulfiqar et al. (2019) used TiO_2 nanoparticles as photocatalysts to degrade the phenol and found that 99.48% of phenol was removed at 1.75 g L^{-1} TiO_2 dose at the 540 min irradiation time.

5.3.6. Kinetic studies of photocatalytic degradation of *p*-cresol by TiO_2 nanoparticle

Fig. 5.4. illustrates the kinetic studies of photocatalytic degradation of *p*-cresol under various concentrations. The linear plot between $ln\frac{C}{C_o}$ and t (irradiation time) and it has been found that for degradation of *p*-cresol, each concentration obeys first-order reaction kinetic. However, *p*-cresol concentration increases (100 mg L^{-1} to 700 mg L^{-1}), the apparent rate **(Fig. 5.4)** constant continuously decreases (0.011 min^{-1} to 0.0005 min^{-1}) and $t_{\frac{1}{2}}$ continuously increases (63.01 min^{-1} to 386.42 min^{-1}) **(Table 5.1.).**

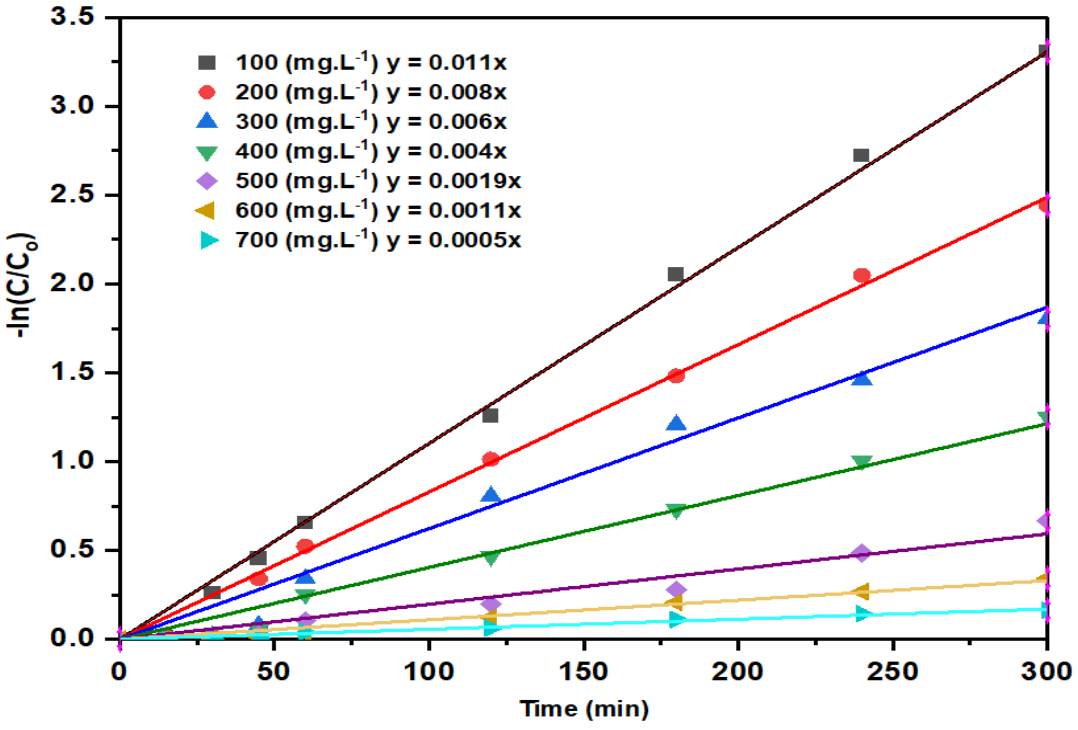

Fig. 5.4. Kinetic of photocatalytic degradation of *p*-cresol using TiO_2 nanoparticle as photocatalyst under UV light

Table 5.1. Pseudo first-order rate constant k_{ap} (min^{-1}) and $t_{\frac{1}{2}}$ min life of *p*-cresol for different concentration

***p-cresol* concentration (mg L^{-1})**	**k_{ap} (min^{-1}) ×10^{-2}**	**R^2**	**$t_{\frac{1}{2}}$ (min) = ($\frac{ln(2)}{K_{ap}}$)**
100	1.1	0.99	63.01
200	0.8	0.98	86.65
300	0.6	0.98	115.53
400	0.4	0.97	173.3
500	0.19	0.98	364.87
600	0.11	0.99	630.19
700	0.05	0.99	1386.42

The decrease in k_{ap} value may be due to the number of *p*-cresol molecules with increasing concentration; however, irradiation time and the total number of active sites per unit photocatalyst mass remain constant. As a result, a decrease in the degradation is observed. Moreover, many *p*-cresol molecules adhere to the photocatalyst catalyst surface at high concentrations, prohibiting light penetrating for photocatalysis. Consequently, the photocatalysts ability to produce holes and electrons for pollutant degradation diminishes (Yang et al., 2022). Gupta et al. (2007) suggested that when the concentration of pollutants increases, the ions of reacting molecules increase between the interlayer spacing of photocatalyst molecules, inhibiting the photocatalytic degradation process by reducing the production of the reactive $OH^{\cdot}$ and $O^{2\cdot}{}_2$ free radicals that are responsible for *p*-cresol degradation. Similar results were found by Nguyen and Juang (2015) for the degradation of p-chlorophenol by hybrid H_2O_2 and TiO_2 in aqueous suspensions under UV irradiation. Melian et al. (2007) used TiO_2 nanoparticles as a photocatalyst to degrade cresol (ortho, meta, and para) and found that the k_{ap} value continuously decreases as concentration increases.

5.3.7. FTIR analysis of undegraded, photocatalytic, photocatalytic and biodegraded samples

FTIR spectroscopy analyses the functional groups and can play a key role in determining the chemical composition of solutions. The presence of main functional groups in undegraded; photocatalytic, photocatalytic and biodegradation samples were qualitatively detected by FTIR between wavenumber ranges of 4000 cm^{-1} to 500 cm^{-1} **(Appendix 5 (f)).** Such bands were

identified at proximately 3448 cm^{-1} (-OH groups in the phenols, carboxylic, or absorbed water), 1630 cm^{-1} (C =O groups in the carboxylic and lactonic groups) (Nguyen et al., 2020). CH_3 bending was identified as the cause of the peaks between 1305 and 1395 cm^{-1} (Singh et al., 2017). The peaks at 1406 cm^{-1} and 1119 cm^{-1} reflect the presence of C=C from stretching the aromatic ring (Yuan et al., 2012) and O-C-O group in the sample (Venugopal et al., 2019). The vibration spectra at 1050 cm^{-1} represent the presence of the $–CH_2–$ group in the sample (Ren et al., 2014). The results of the FTIR analysis demonstrated that *p*-cresol was degraded into various intermediate products by combining the photocatalytic reactor with the bioreactor **(Appendix 5 (f)).**

5.3.8. Photocatalytic and biodegradation of *p*-cresol

The % removal of *p*-cresol photocatalytic followed by biodegradation is illustrated in **Fig. 5.5.** Jamil et al. (2011) reported a low biodegradability index (BOD_5/COD (<0.3)), indicating that wastewater does not have a higher ability for biodegradation. To enhance the biodegradability of *p*-cresol (700 mg L^{-1}), wastewater was fed into the photocatalytic reactor (300 min), and then the partially oxidized solution was fed into a fixed bed bioreactor. To assess the performance of the packed bed biofilm reactor, it was operated without pre-oxidized *p*-cresol solution (700 mg L^{-1}). **Fig. 5.5.** shows that the maximum % RE_p (without pre-oxidized) in fixed bed bioreactor was 34.82±2.31%. This might be attributed to the low biodegradability index (BOD/COD< 0.3) of *p*-cresol. However, when the pre-oxidized solution was used in the packed bed biofilm reactor, the maximum % removal (for the same fixed retention time of 120 h) was 98.43±1.31%. On the other hand, increase in % removal of *p*-cresol may be due to photocatalysis reduced *p*-cresol inhibition effect on biomass and degraded *p*-cresol to biodegradable intermediates for biofilm utilization.

5.3.9. Performance assessment of packed bed biofilm reactor

The performance of a continuous PBBR for the fixed concentration of *p*-cresol (700 mg L^{-1}) and various flow rates (20-, 40, and 60 mL h^{-1}) was investigated **(Fig. 5.6.).** For each flow rate, several parameters, such as % removal efficiency (REp), pollutant loading rate (PLR), and elimination capacity (ECPR), were evaluated. The maximum % REp was 60.69% at PLR 336 mg L^{-1} d^{-1} after 10 days operation with ECPR 203.93 mg $L^{-1}d^{-1}$ **(Fig. 5.6.).** When the flow rates

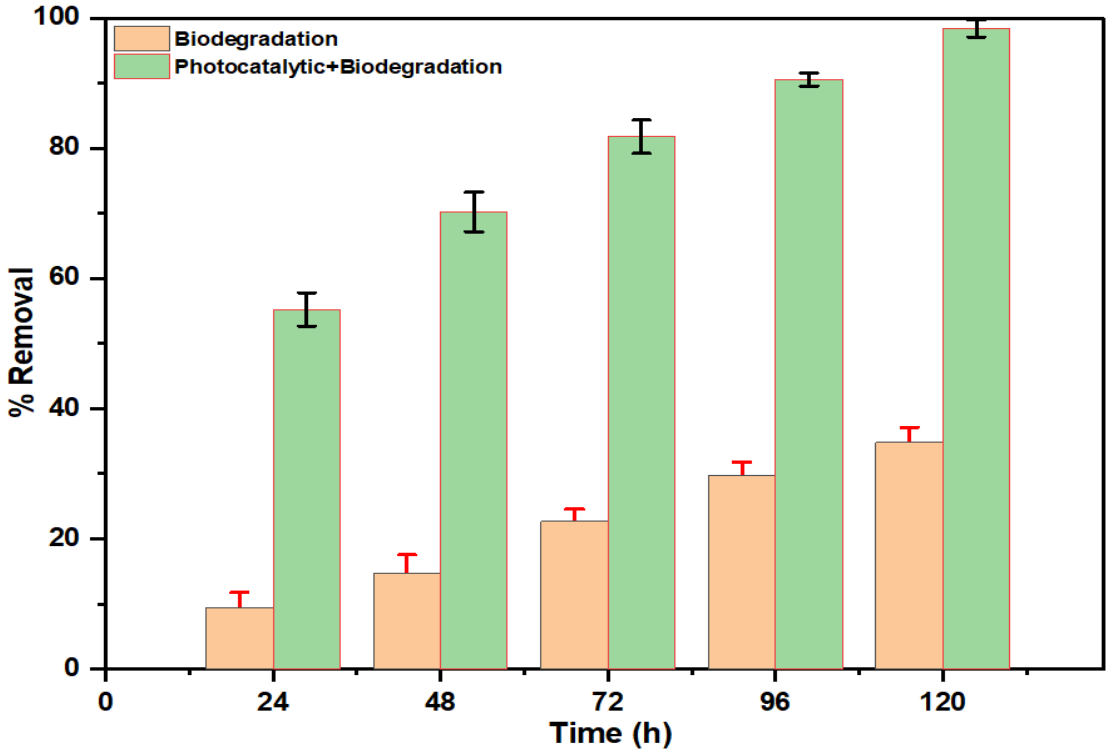

Fig. 5.5. Comparative study of % removal of *p*-cresol (700 mg L^{-1}) in pure biodegradation and photocatalytic combined with biodegradation at optimized conditions

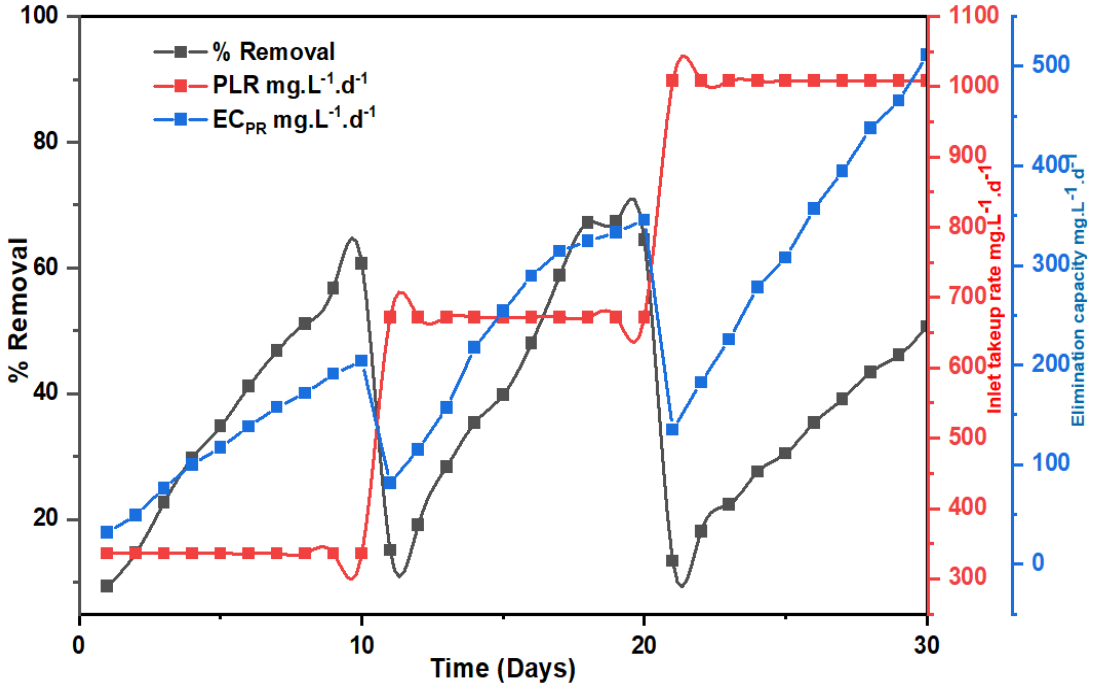

Fig 5.6. Impact of pollutant loading rate % removal of *p*-cresol and elimination capacity of PBBR

were raised from 20 mL h^{-1} to 40 mL h^{-1}, on the 11th day, % REp was 60.69 % to 65.32%. This may be because, at low loading rates, the biofilm acts as diffusional resistance, lowering the permeability of pollutants toward the inner shell biofilm. In this circumstance, the innermost layer of the biofilm, which is close to the surface of the packing media, won't have enough substrate, and the microbes' ability to degrade the pollutant won't be fully utilized (Banerjee and Ghoshal, 2016). However, the flow rate was raised from 40 mL h^{-1} to 60 mL h^{-1} on the 21st day of operation; the RE_p decreased from 60.39 % to 50.69%, corresponding to PLR and ECPR 1008 mg $L^{-1}d^{-1}$, 511.02 mg $L^{-1}d^{-1}$ respectively. The decrease in RE_p at higher feed flow rates was caused by a shorter contact period time between the immobilized cell and the substrate. According to the observations, using solid supports with porous structures and high water-holding resistance, such as PUF, increases the contact between pollutants and microorganisms, allowing a reasonable biodegradation rate even in the case of low biodegradable pollutants.

5.3.10. Growth and inhibition kinetics model

The Monod and Andrew-Haldane models were used to understand the kinetic parameters for substrate inhibition and non-inhibition accordingly. It was observed that maximum specific growth (μ) was 0.18±0.003 h^{-1} at 100 mg L^{-1} *p*-cresol concentration **(Appendix 5 (g)).** However, a further increase in *p*-cresol concentration (100 mg L^{-1} to 700 mg L^{-1}) decreases the specific growth (0.12±0.01 h^{-1} to 0.010±0.01 h^{-1}). These results reflect increasing *p*-cresol concentration from 100 mg L^{-1} to 700 mg L^{-1} biodegradation was inhibited. Based on the Andrew-Haldane model, biokinetic parameters such as maximum specific growth rate (μ_{max}), half-saturation constant (K_s) and substrate inhibition constant (K_I) was obtained as 0.20±0.01 h^{-1}, 75.83 ±0.01 mg L^{-1} and 150 mg L^{-1}, respectively. When there is inhibition, it is better to use the maximum feasible specific *p*-cresol biodegradation rate $\hat{q}$, which, based on the kinetic model **(Eq. (5.11)),** is 0.13±0.01 (h^{-1}) at a *p*-cresol concentration of 100 mg L^{-1}. To quantify the degradation potential of microorganisms, the $\frac{\mu_{max}}{K_I}$ value has been widely accepted as an essential parameter (Kureel et al., 2017) was to be 1.33×10^3 h^{-1} mg^{-1} L. Bera et al. (2019) isolated *Stenotrophomonas sp*. from petroleum refinery wastewater to degrade *p*-cresol (100 mg L^{-1}). They found Andrew-Haldane model was comparable to the observed (Experimental) results with kinetics growth parameters μ_{max} specific growth 0.116 h^{-1}, substrate growth inhibition constant K_I =387 mg L^{-1}.

5.4. Conclusions

This study illuminates that an integrated system is beneficial for degrading high-concentration of *p*-cresol solutions. The % removal efficiency of *p*-cresol through an integrated system was much better than a packed bed biofilm reactor operated separately. On the increase in p- cresol concentration, the pseudo-first-order rate constant (K_{ap}) continuously decreases. Andrew-Haldane biodegradation growth kinetic models were followed. An integrated system (photocatalysis combined with biodegradation) offers effective and sustainable pollutant degradation and mitigation techniques. Its scalability, synergistic advantages and flexibility make it the benchmark among emerging technologies. The integrated system can further be extended to treat a wide range of recalcitrant pollutants.